



Crystal structure, magnetic properties and Mössbauer studies of $[\text{Fe}(\text{qsal})_2][\text{Ni}(\text{dmit})_2]$

Christophe Faulmann ^{a,*}, Stéphane Dorbes ^a, Stéphane Lampert ^a, Kane Jacob ^a,
Bénédicte Garreau de Bonneval ^a, Gábor Molnár ^a, Azzedine Bousseksou ^a,
José Antonio Real ^b, Lydie Valade ^a

^a Laboratoire de Chimie de Coordination, 205 Route de Narbonne, 31077 Toulouse Cedex, France

^b Institut de Ciencia Molecular, Departament de Química Inorgànica, Universitat de València, Edificio de Institutos de Paterna, P.O. Box 22085, 46071 Valencia, Spain

Received 21 November 2006; received in revised form 2 March 2007; accepted 7 March 2007

Available online 21 March 2007

Paper presented in the MAGMANet-ECMM, European Conference on Molecular Magnetism.

Abstract

A new compound of formula $[\text{Fe}(\text{qsal})_2][\text{Ni}(\text{dmit})_2]$ (**1**) has been synthesised, structurally and magnetically characterised (qsalH = *N*-(8-quinolyl)salicylaldimine, dmit^{2-} = 1,3-dithiol-2-thione-4,5-dithiolato). Its structural features and its magnetic behaviour were compared with those of $[\text{Fe}(\text{qsal})_2]$ -based complexes, and more particularly $[\text{Fe}(\text{qsal})_2][\text{Ni}(\text{dmit})_2] \cdot 2\text{CH}_3\text{CN}$.
© 2007 Elsevier B.V. All rights reserved.

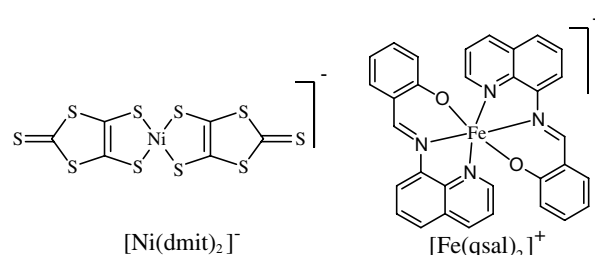
Keywords: X-ray crystal structures; Mossbauer spectroscopy; Spin crossover; Metal bisdithiolene complex; Magnetic properties; Pressure effects

1. Introduction

The design and preparation of materials based on transition metal building blocks and displaying a switching behaviour, i.e. spin crossover (SC), is an area of intense interest [1,2]. Indeed, such systems can act as active elements in switches, display and memory devices [3]. Molecular compounds derived from metal bisdithiolene can also act as sensors and exhibit remarkable properties such as (super)conductivity, but also various magnetic and optical phenomena [4].

We decided to combine SC systems with the $\text{Ni}(\text{dmit})_2$ unit (dmit^{2-} : 2-thio-1,3-dithiole-4,5-dithiolato), well known for its conductive properties when in a fractional oxidation state [4,5]. The ultimate objective is to develop multi-property materials exhibiting novel physical proper-

ties, due to the possible synergy between the physical properties carried by each building block.



Very recently, we have reported [6] the new SC complex $[\text{Fe}(\text{sal}_2\text{-trien})][\text{Ni}(\text{dmit})_2]$, which exhibits a wide thermal hysteresis loop of its magnetic susceptibility. Such a behaviour is quite unusual for Fe(III) complexes [7]. It might be due to the particular arrangement of the crystal packing, which favours the occurrence of segregated stacks of

* Corresponding author. Tel.: +33 5 6133 3122; fax: +33 5 6155 3003.
E-mail address: faulmann@lcc-toulouse.fr (C. Faulmann).

cations and anions with a large number of short interactions between them, among which are π – π contacts between aromatic rings of the ligands. In the same line, we have decided to work with the $[\text{Fe}(\text{qsal})_2]^+$ cation ($\text{qsalH} = N$ -(8-quinolyl)salicylaldimine), obtained originally as the chlorine salt [8]. The qsal ligand contains several aromatic rings, which might interact through π – π contacts. Indeed, such interactions are observed within the few complexes (only 9) based on this cation [9–14]. All of them but two (I- and Br-derivatives [9]) exhibit spin transition. For $[\text{Fe}(\text{qsal})_2]\text{NCS}$ [9,10], a spin-crossover behaviour is reported together with a hysteresis loop. The $[\text{Fe}(\text{qsal})_2]\text{NCSe} \cdot \text{solvent}$ (solvent = CH_2Cl_2 , MeOH, 2DMSO) [11,12] complexes show a complete spin transition accompanied with an apparent hysteresis, due to desolvation. More recently, Takahashi et al. reported two complexes combining the $[\text{Fe}(\text{qsal})_2]^+$ cation and the $[\text{Ni}(\text{dmit})_2]^-$ anion, namely $[\text{Fe}(\text{qsal})_2][\text{Ni}(\text{dmit})_2] \cdot 2\text{CH}_3\text{CN}$ [13] and $[\text{Fe}(\text{qsal})_2][\text{Ni}(\text{dmit})_2]_3 \cdot \text{CH}_3\text{CN} \cdot \text{H}_2\text{O}$ [14]. Spin transition is observed in both of them, and they also exhibit Light Induced Excited Spin State Trapping effect (LIESST). This is of particular interest in the SCO complexes, since it could allow obtaining photo-switchable molecular materials.

We report herein the preparation and structural and magnetic characterisations of the new complex $[\text{Fe}(\text{qsal})_2][\text{Ni}(\text{dmit})_2]$ (**1**), which is not solvated in contrast to $[\text{Fe}(\text{qsal})_2][\text{Ni}(\text{dmit})_2] \cdot 2\text{CH}_3\text{CN}$ [13]. The lack of solvent induces a different crystal structure, together with a different magnetic behaviour.

2. Experimental

2.1. General remarks

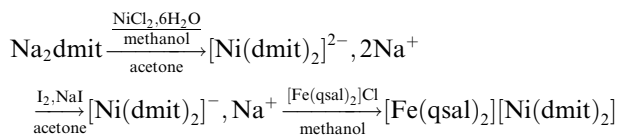
All solvents were dried and distilled under argon atmosphere prior to use. All syntheses were carried out in an inert atmosphere glove box or using the Schlenk techniques. $[\text{Fe}(\text{qsal})_2]\text{Cl} \cdot 1.5\text{H}_2\text{O}$ and $(n\text{-Bu}_4\text{N})[\text{Ni}(\text{dmit})_2]$, (tetrabutylammonium bis(1,3-dithiol-2-thione-4,5-dithiolato) nickelate(III)) were synthesized following literature procedures reported by Dickinson and coworkers [9] and Steimecke and coworkers [15], respectively.

2.2. Synthesis of the $[\text{Fe}(\text{qsal})_2][\text{Ni}(\text{dmit})_2]$ complex (**1**)

- (a) $[\text{Fe}(\text{qsal})_2]\text{Cl} \cdot 1.5\text{H}_2\text{O}$ (123 mg, 0.20 mmol) is dissolved in an acetone/methanol solution (20 mL/20 mL) in an ultrasonic bath for 30 min. This solution is then slowly added to an acetone solution of $(n\text{-Bu}_4\text{N})[\text{Ni}(\text{dmit})_2]$ (159 mg, 0.23 mmol). After elimination by filtration of $(n\text{-Bu}_4\text{N})\text{Cl}$ which forms immediately, the filtrate is placed at 4 °C overnight. After filtration, a grey-black microcrystalline powder is harvested, washed several times with acetone and

dried under vacuum. Yield: 86 mg (43%). *Elemental Anal.* Calc. for $[\text{Fe}(\text{qsal})_2][\text{Ni}(\text{dmit})_2]$ ($\text{C}_{38}\text{H}_{22}\text{FeN}_4\text{NiO}_2\text{S}_{10}$) (**1**): C, 45.56; H, 2.21; N, 5.59. Found: C, 44.28; H, 1.94; N, 5.08%.

- (b) Compound **1** can also be obtained by using the “ dmitNa_2 ” method [16].



dmitNa_2 (125 mg, 0.52 mmol) is dissolved in 24 mL of acetone. 61.6 mg (0.25 mmol) of $\text{NiCl}_2 \cdot 6\text{H}_2\text{O}$ in 2.26 mL of methanol is added dropwise to the obtained dark purple solution. $\text{Na}_2[\text{Ni}(\text{dmit})_2]$ remains in solution and is then oxidized by addition of an acetone solution (60 mL) of I_2 (32.9 mg, 0.13 mmol) and NaI (153.2 mg, 0.26 mmol). $\text{Na}[\text{Ni}(\text{dmit})_2]$ also remains in solution. A solution of $[\text{Fe}(\text{qsal})_2]\text{Cl} \cdot 1.5\text{H}_2\text{O}$ (153 mg, 0.25 mmol) dissolved in 38 mL of MeOH is then added dropwise. The resulting solution is evaporated (half-volume). Isopropanol is added and the solution is left at 4 °C overnight. After filtration, the grey-black microcrystalline powder is washed with cold methanol and dried under vacuum. Yield: 186 mg (72%). *Elemental Anal.* Calc. for $[\text{Fe}(\text{qsal})_2][\text{Ni}(\text{dmit})_2]$ ($\text{C}_{38}\text{H}_{22}\text{FeN}_4\text{NiO}_2\text{S}_{10}$) (**1**): C, 45.56; H, 2.21; N, 5.59. Found: C, 44.65; H, 1.87; N, 4.98%.

Single crystals of **1** were obtained by metathesis reaction from $[\text{Fe}(\text{qsal})_2]\text{Cl} \cdot 1.5\text{H}_2\text{O}$ and $(n\text{-Bu}_4\text{N})[\text{Ni}(\text{dmit})_2]$, using a diffusion cell equipped with three compartments separated with glass-frits. After ca. 10 days, brown bar-shaped single crystals were harvested and characterised by X-ray diffraction.

2.3. Physical measurements

2.3.1. Magnetic measurements

Magnetic studies were performed on polycrystalline powders, between 2 and 300 K. Magnetic susceptibility measurements were carried out with a Quantum Design MPMS 5 magnetometer with an applied field of 10 kOe and 500 Oe at low temperature. The independence of the susceptibility value with respect to the applied field was checked at room temperature. The susceptibility data were corrected from the diamagnetic contributions.

Magnetic susceptibility measurements at high pressures have been carried out in 20 kOe magnetic field using a clamp-type, hardened beryllium bronze (CuBe) cell [17]. Hydrostatic conditions were obtained by mixing the powder samples (ca. 15 mg) with a pressure transmitting mineral oil (Alcatel-100). The pressure inside the cell was determined with an accuracy of ± 0.015 GPa from the pressure shift of the superconducting transition of a 99.99% purity Pb wire. The hydrostatic conditions at high

pressures and low temperatures were maintained as inferred from the abruptness of the lead superconducting transition. The temperature cycles were carried out at a rate of 1 K min⁻¹, the pressure was clamped at a fixed value at room temperature. The contribution from the pressure cell to the total susceptibility was subtracted by carrying out dummy runs.

2.3.2. Mössbauer experiments

The variable temperature ⁵⁷Fe Mössbauer measurements were carried out by means of a conventional con-

Table 1
Crystal data and structure refinement for **1** at 290, 180 and 100 K

	[Fe(qsal) ₂][Ni(dmit) ₂] (1)		
Empirical formula	C ₃₈ H ₂₂ FeN ₄ NiO ₂ S ₁₀		
Formula weight	1001.76		
<i>T</i> (K)	290	180	100
Wavelength (Å)	0.71073		
Crystal system	triclinic		
Space group	P $\bar{1}$		
<i>Unit cell dimensions</i>			
<i>a</i> (Å)	9.4010(13)	9.4099(9)	9.4129(11)
<i>b</i> (Å)	12.3537(15)	12.2921(13)	12.2518(14)
<i>c</i> (Å)	19.558(3)	19.502(2)	19.4560(23)
α (°)	72.229(10)	71.709(13)	71.511(14)
β (°)	86.058(13)	85.759(13)	85.724(14)
γ (°)	69.380(12)	68.821(12)	68.466(13)
<i>V</i> (Å ³)	2022.5(5)	1995.1(4)	1977.2(4)
<i>Z</i>	2		
ρ_{calc} (Mg/m ³)	1.645	1.667	1.683
μ (mm ⁻¹)	1.382	1.401	1.414
<i>F</i> (000)	1016		
Crystal size (mm)	0.60 × 0.33 × 0.10	0.44 × 0.16 × 0.12	0.60 × 0.33 × 0.10
θ Range for data collection (°)	3.26–32.18	2.20–25.94	2.20–25.83
<i>Index ranges</i>			
<i>h</i>	–11, 13	–11, 11	–11, 11
<i>k</i>	–17, 18	–15, 15	–14, 14
<i>l</i>	–28, 29	–24, 23	–23, 23
Reflections collected	2262	1928	19367
Independent reflections [<i>R</i> _{int}]	128835 [0.0652]	7208 [0.0826]	7131 [0.0521]
Completeness to θ	90.3% at $\theta_{\text{max}} = 32.18^\circ$	92.5% at $\theta_{\text{max}} = 25.94^\circ$	92.6% at $\theta_{\text{max}} = 25.91^\circ$
Absorption correction	GAUSSIAN		
Refinement method	full-matrix least-squares on <i>F</i> ²		
Data/restraints/parameters	12883/0/508	7208/4/508	7131/4/508
Goodness-of-fit on <i>F</i> ²	0.831	0.947	1.079
Final <i>R</i> indices [<i>I</i> > 2 σ (<i>I</i>)]	<i>R</i> ₁ = 0.0622, <i>wR</i> ₂ = 0.1545	<i>R</i> ₁ = 0.0557, <i>wR</i> ₂ = 0.1214	<i>R</i> ₁ = 0.0662, <i>wR</i> ₂ = 0.1552
<i>R</i> indices (all data)	<i>R</i> ₁ = 0.1530, <i>wR</i> ₂ = 0.1922	<i>R</i> ₁ = 0.1069, <i>wR</i> ₂ = 0.1388	<i>R</i> ₁ = 0.0800, <i>wR</i> ₂ = 0.1630
Largest difference in peak and hole (e ⁻ Å ⁻³)	0.612 and –0.527	0.843 and –0.493	1.285 and –1.206

$$R_1 = \sum \|F_o\| - |F_c| / \sum |F_o|; wR_2 = \{ \sum [w(F_o^2 - F_c^2)^2] / \sum [w(F_o^2)^2] \}^{1/2}.$$

$S = \{ \sum [w(F_o^2 - F_c^2)^2] / (n - p) \}^{1/2}$ where *n* is the number of reflections and *p* is the total number of parameters refined. $w = 1 / [\sigma^2(F_o^2) + (aP)^2 + bP]$ avec $P = [2F_c^2 + \text{Max}(F_o^2, 0)] / 3$.

stant-acceleration spectrometer with a 50 mCi ⁵⁷Co(Rh) source on ca. 60 mg powder sample enclosed in a 12 mm diameter cylindrical plastic sample holder. The samples were cooled down in a custom-designed, liquid helium flow-type cryostat. A least-squares computer program was used to fit the Mössbauer parameters and to determine the standard deviations of statistical origin [18]. The isomer shift values are given with respect to metallic iron at room temperature.

2.3.3. X-ray crystallographic study on single crystals

The experimental details and crystal data are listed in Table 1. Data collection and cell refinement were performed with a sealed Mo K α ($\lambda = 0.71073$ Å) X-ray source on a Stoe Imaging Plate Diffraction System (IPDS) diffractometer, by using the IPDS software [19] at 180 and 100 K, and on an Oxford Xcalibur diffractometer, by using the CRYSLIS softwares [20,21] at 290 K. Crystal decay was monitored by measuring a maximum of 200 reflections per image (Stoe diffractometer) or several test reflections (Xcalibur diffractometer). The structures were solved using SIR97 [22] or SHELXS97 [23] and refined using SHELXL97 [24] for subsequent refinement. The calculations were carried out with the WINGX program package [25]. The drawings of the molecular structures were performed with CAMERON [26] and ORTEP [27]. The atomic scattering factors were taken from the International tables for X-ray crystallography [28].

3. Results and discussion

3.1. Magnetic properties of **1**

The temperature dependence of the $\chi_M T$ product is shown in Fig. 1. At room temperature, the $\chi_M T$ product is 5.04 cm³ K mol⁻¹, a value which agrees quite well with that expected for the sum of the $\chi_M T$ of a Fe^{III} ion in the high-spin (HS) state (*S* = 5/2, *g* \approx 2.05) and a [Ni(dmit)₂]⁻ radical (*S* = 1/2, *g* \approx 2.19). At 300 K the system is therefore purely HS. The $\chi_M T$ value slowly decreases down to ca. 2 K, but not in a regular way. Between 300 and 220 K (zone a), the $\chi_M T$ product decreases only slightly (from 5.04 to 4.51 cm³ K mol⁻¹). In zone b (220–70 K), the decreasing is more important (from 4.51 down to 2.89 cm³ K mol⁻¹). Between 70 and 30 K, the decreasing is almost similar to that observed in zone a. From 30 K down to 2 K, the decreasing is very large (from 2.58 to 1.77 cm³ K mol⁻¹), and might be due to the zero field-splitting and/or intermolecular magnetic coupling. At 2 K, the $\chi_M T$ product is larger than the expected value for a Fe^{III} in the low-spin (LS) state. These results indicate that from room temperature down to 2 K, the Fe^{III} ions in this complex exhibit a gradual and incomplete *S* = 5/2 \rightarrow *S* = 1/2 spin state change. The magnetic behaviour is the same upon cooling and heating, indicating that there is no hysteresis loop.

To verify the occurrence of spin crossover and the above interpretation of the magnetic behaviour as well

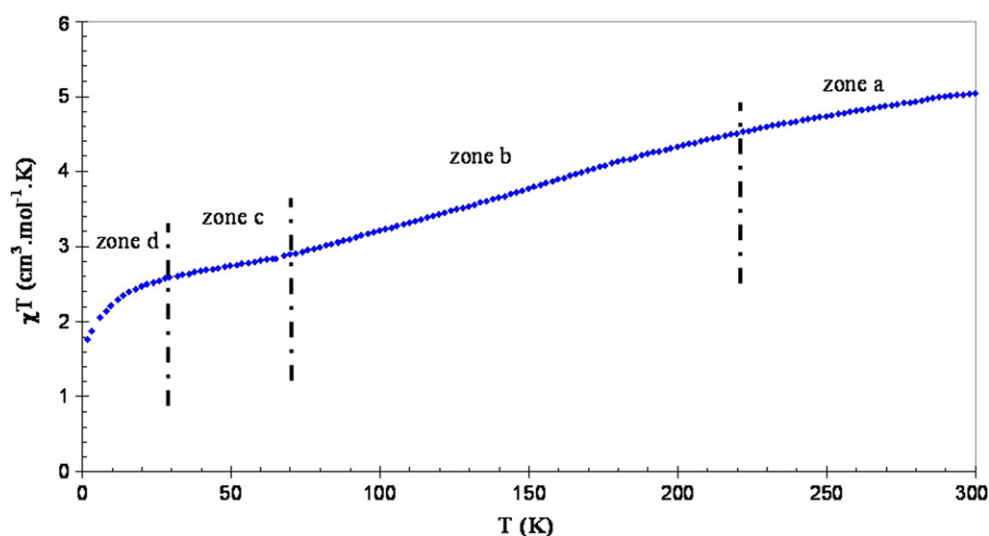


Fig. 1. Temperature dependence of the magnetic susceptibility for **1** at atmospheric pressure.

as to determine the residual HS fraction, Mössbauer spectra of **1** have been recorded at some representative temperatures (Fig. 2, Table 2). At 293 K the spectrum displays only one doublet with isomer shift (δ) of $0.36(1) \text{ mm s}^{-1}$ and quadrupole splitting (ΔE_Q) of $0.23(2) \text{ mm s}^{-1}$ values, in agreement with the presence of pure HS Fe^{III} form ($S = 5/2$). The slight asymmetry of this doublet may be due to texture effect as it persists when the temperature is decreased. At 80 K, the Mössbauer spectrum consists of two distinct doublets with an area ratio $A_{\text{HS}}/A_{\text{tot}}$ of *ca.* 52 %, which is in good agreement with the magnetic data. The distinct spectra without any line broadening observed for the two spin-states indicate that the spin inter-conversion rates are slow compared to the hyperfine frequencies of Mössbauer spectroscopy (*ca.* 10^7 s^{-1}). The second doublet shows

large quadrupole splitting (Table 2) as expected for the $S = 1/2$ spin state of LS Fe^{III} ions. Upon further decrease of the temperature, the spin fractions remain stable as can be inferred from the 4 K spectrum ($A_{\text{HS}}/A_{\text{tot}} = 55\%$), indicating that the decrease of the $\chi_{\text{M}}T$ value below 80 K is indeed due to the zero-field splitting of HS Fe^{III} ions.

This largely incomplete and progressive transition, as well as the slight increase of the HS fraction at low temperatures, is reminiscent of the behaviour of the complexes $[\text{Fe}(\text{TRIM})_2]\text{F}_2$ and $[\text{Fe}(\text{3OMe}, \text{5NO}_2\text{-sal-N}(1,10)\text{-NMe}(4,7))]$, whose HS and LS states are almost “equi-energetic” [29–32]. In fact, in spin crossover systems characterized by a low equilibrium temperature $T_{1/2}$, *i.e.* a small energy gap between the LS and HS states, the thermal population of vibrational levels will

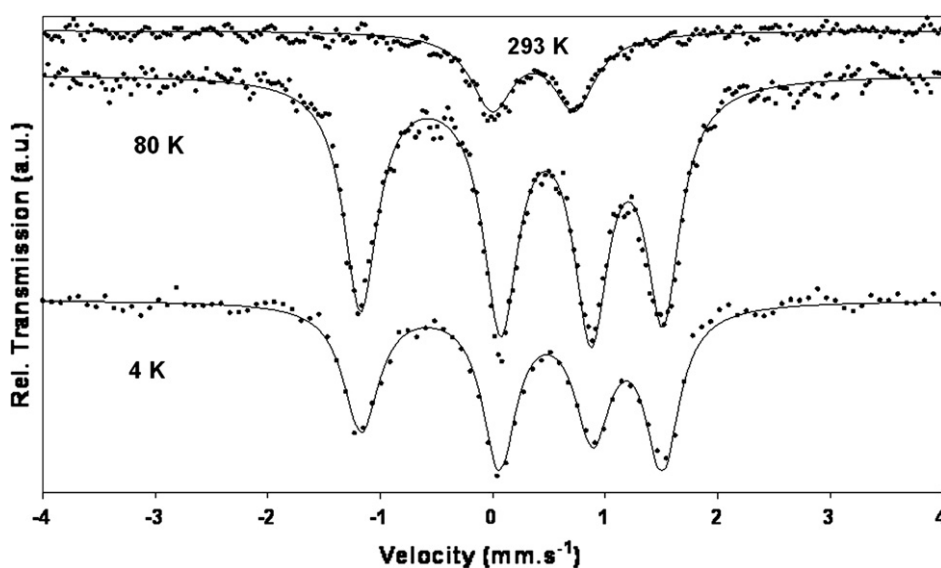


Fig. 2. Representative Mössbauer spectra of **1**.

Table 2
Least-squares-fitted Mössbauer data for **1**

T (K)	Low-spin			High-spin			$A_{\text{HS}}/A_{\text{tot}}$
	δ (mm/s)	ΔE_{Q} (mm/s)	$\Gamma/2$ (mm/s)	δ (mm/s)	ΔE_{Q} (mm/s)	$\Gamma/2$ (mm/s)	
4	0.17(1)	2.69(1)	0.17(2)	0.48(1)	0.85(2)	0.20(2)	0.55(1)
80	0.17(1)	2.69(1)	0.18(1)	0.472(7)	0.80(1)	0.190(9)	0.52(1)
293				0.36(1)	0.73(1)	0.23(2)	1

δ , isomer shift; ΔE_{Q} , quadrupole splitting; Γ , half-height width of the line; $A_{\text{HS}}/A_{\text{tot}}$, area ratio (error bars are given in parentheses and isomer shift values refer to metallic iron at room temperature).

govern the spin crossover at sufficiently low temperatures and this type of situation may even lead to a change in the nature of the ground state. However, this change is usually completely masked in the magnetic measurements by the zero-field splitting effect. On the other hand, Mössbauer spectra are not hampered with this effect and therefore Mössbauer spectroscopy is a more convenient way for the analysis of the temperature dependence of spin fractions in this temperature range. As discussed in Ref. [18], the observation of an increase of the HS fraction upon decreasing temperature is an indication for such “equi-energetic” situation. Indeed, Mössbauer spectra of **1** reveal a slight increase of the HS fraction when going from 80 to 4 K, but the change (3%) is very close to the experimental uncertainties. One should also consider that kinetic is very slow at these temperatures (“freezing” of the spin conversion) and the equilibrium population of levels cannot be achieved. To investigate systems with small energy gap and to avoid freezing effects, one may apply external pressure, which increases the gap between the zero point energies by the work term $P\Delta V_{\text{HL}}$ (where $\Delta V_{\text{HL}} > 0$ is the volume difference

between the HS and LS states). Pressure will thus stabilize the LS state and shift the transition to higher temperatures where no freezing occurs. Therefore, the transition becomes more complete. Several examples for this type of pressure effect were reported by Ksenofontov et al. [33]. In order to try to convert the low-temperature HS fraction into the LS state external, pressure was thus applied on sample **1** and the magnetic susceptibility was determined under pressure as a function of temperature. Fig. 3 shows the $\chi_{\text{m}}T$ product as a function of temperature in the cooling mode at different applied pressures. As expected, with increasing pressures, the transition shifts to higher temperatures. On the other hand, the shape of the transition curve does not change significantly and the low-temperature HS fraction decreases only slightly. From this observation, we infer that the low-temperature residual fraction is not related to freezing effects. This HS residue at low temperatures probably results from a part of the molecules located at some lattice site where the ligand-field strength is reduced (due to crystal defects, etc.) to prevent the formation of low spin molecules.

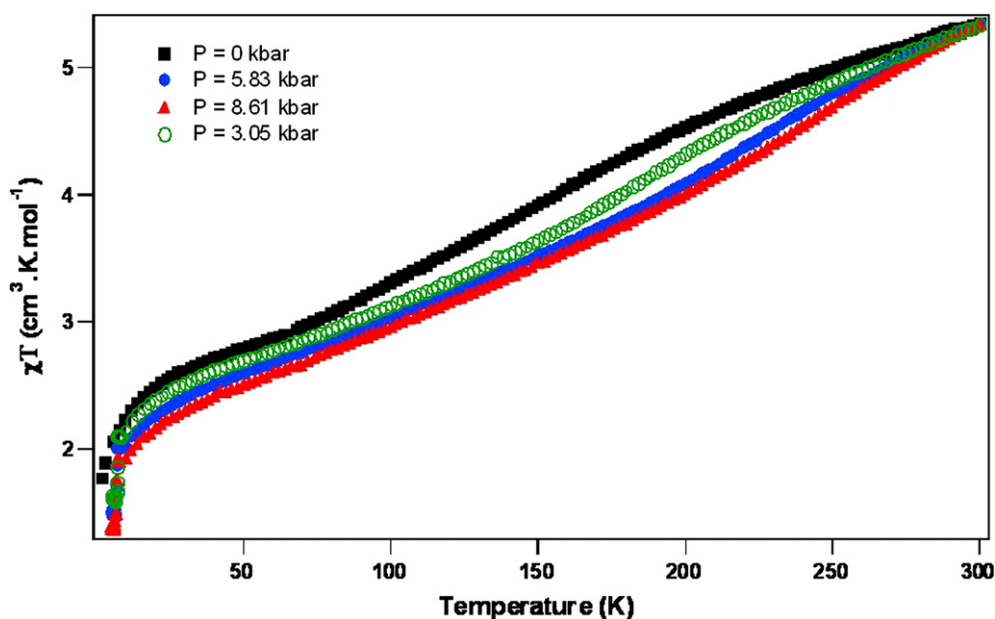


Fig. 3. Temperature dependence of the $\chi_{\text{M}}T$ product for **1** at different applied pressures.

3.2. Description of the structure of **1**

The asymmetric unit of **1** contains one $[\text{Fe}(\text{qsal})_2]^+$ cation and two halves of $[\text{Ni}(\text{dmit})_2]^-$ anion, each Ni atom lying on a centre of inversion (Fig. 4).

Whatever the temperature, the structure is built on layers of $[\text{Ni}(\text{dmit})_2]^-$ alternating with “mixed” layers of $[\text{Fe}(\text{qsal})_2]^+$ and $[\text{Ni}(\text{dmit})_2]^-$. These layers spread onto the *ab* plane and are perpendicular to the *ac* plane. Short contacts (smaller than the sum of the van der Waals radii of the concerned atoms [34]) between molecular units are observed within and between these layers. (Fig. 5).

The mixed layers of $[\text{Fe}(\text{qsal})_2]^+$ and $[\text{Ni}(\text{dmit})_2]^-$ are shown on Fig. 6, left. In these layers, one can observe a

stacking of the $[\text{Fe}(\text{qsal})_2]^+$ cations along the *a* direction, which then form a network of parallel chains. The interactions within and between the chains only appear between perpendicular ligands (Fig. 6, right), without any π - π interaction.

Coordination bond lengths around the Fe atom are shown in Table 3. The Fe atom lies in an octahedral environment, and is bonded to two *qsal*⁻ ligands (hereafter noted A and B), through two oxygen atoms (O1 and O2), two imine-nitrogen atoms (N1 and N3) and two quinoline-nitrogen atoms (N2 and N4). When the temperature decreases, the bond lengths become more homogeneous and the octahedron around the Fe atom is more regular: this is in agreement with the occurrence of a

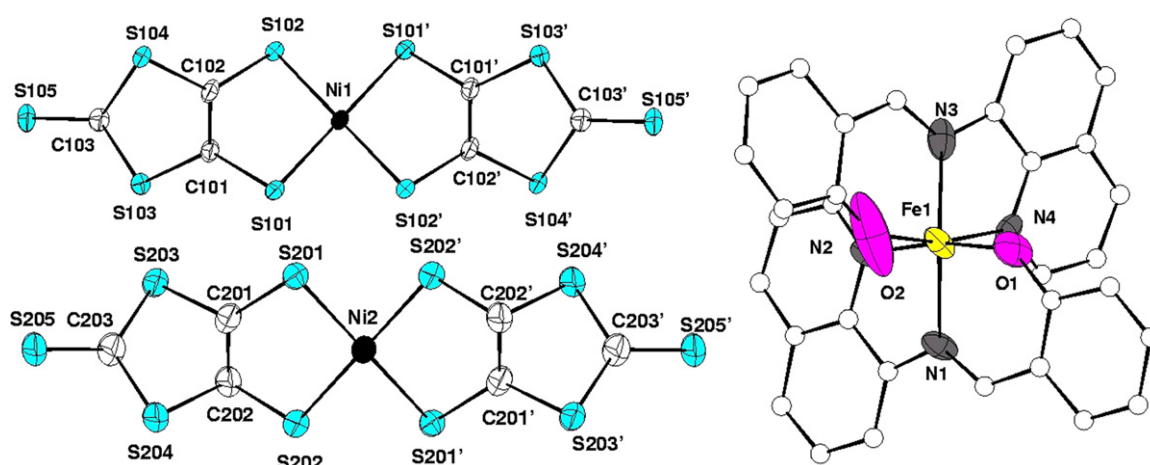


Fig. 4. Atomic numbering scheme for **1**.

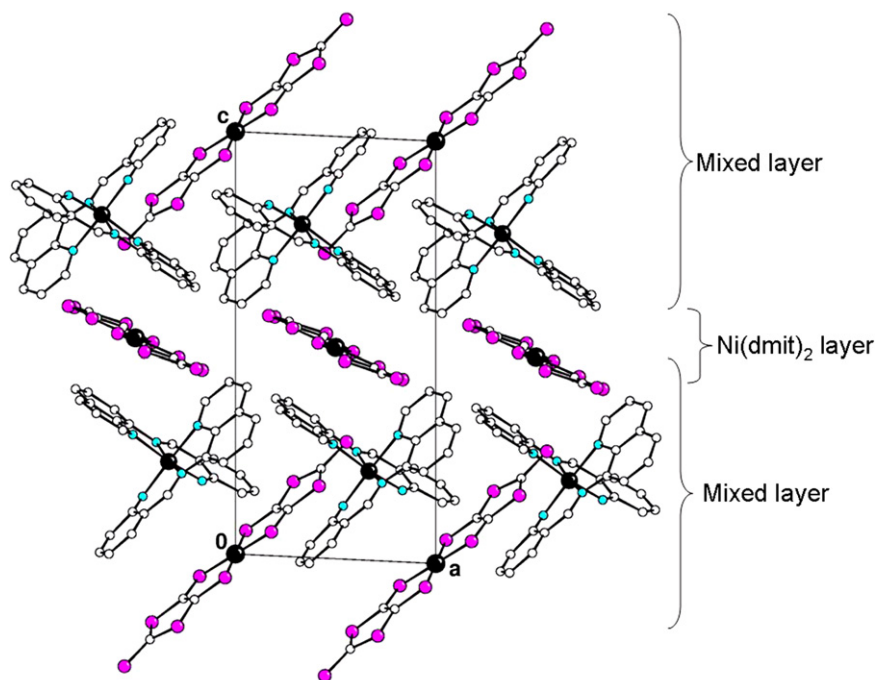


Fig. 5. View of the structural arrangement of **1** along the *b* direction.

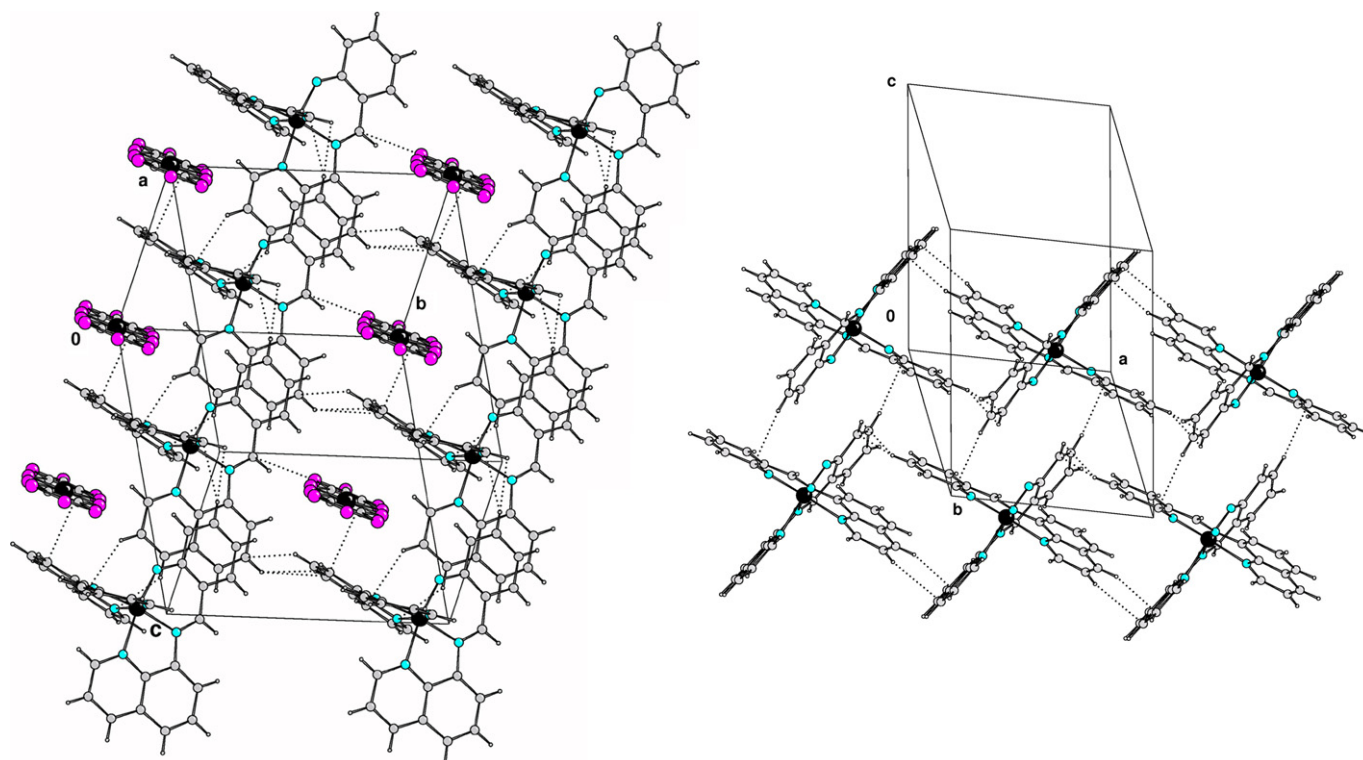


Fig. 6. Mixed layers of $[\text{Ni}(\text{dmit})_2]^-$ and $[\text{Fe}(\text{qsal})_2]^+$ in **1** (left) and stacking of the $[\text{Fe}(\text{qsal})_2]^+$ cations along the a direction (right).

Table 3
Bond lengths around Fe in **1**

Bond	Bond length (Å)		
	$T = 300 \text{ K}$	$T = 180 \text{ K}$	$T = 100 \text{ K}$
<i>Ligand A</i>			
Fe1–O1	1.897	1.885	1.885
Fe1–N1	2.103	2.074	2.047
Fe1–N2	2.109	2.079	2.055
<i>Ligand B</i>			
Fe1–O2	1.907	1.913	1.900
Fe1–N3	2.108	2.069	2.038
Fe1–N4	2.123	2.098	2.069

spin crossover from the HS state to the LS state (see below).

Whatever be the temperature and the ligand (A or B), the Fe–O lengths are the shortest. For a given temperature, in ligand A, the Fe–N bond lengths are almost similar, whatever be the nature of the N atom (imine or quinoline). This is not the case for ligand B, since large discrepancies are observed between Fe1–N3 and Fe1–N4, the bond involving the quinoline atom being always longer.

These differences in ligands A and B are also reflected by the values of the angles between the phenyl ring and the quinoline ring of the qsal ligand. Since these aromatic rings are connected through an imine bond, they should lie more or less in the same plane. This is almost true for ligand A (angles ranging between 8.69° and 9.44°), but a large distortion is observed in the case of ligand B since these rings form angles of *ca.* 20° (Table 4).

Table 4
Angle between the phenyl and quinoline rings in **1** at 300, 180 and 100 K

Temperature (K)	Angle ($^\circ$)	
	Ligand A	Ligand B
300	8.69	19.26
180	9.38	19.80
100	9.44	18.08

Among the few $[\text{Fe}(\text{qsal})_2]$ -based complexes reported in the literature [9–14], only two contain the $\text{Ni}(\text{dmit})_2$ unit, namely $[\text{Fe}(\text{qsal})_2][\text{Ni}(\text{dmit})_2] \cdot 2\text{CH}_3\text{CN}$ [13] and $[\text{Fe}(\text{qsal})_2][\text{Ni}(\text{dmit})_2]_3 \cdot \text{CH}_3\text{CN} \cdot \text{H}_2\text{O}$ [14]. The latter is a fractional oxidation state complex, whose crystal structure is built on segregated layers of $[\text{Fe}(\text{qsal})_2]^+$ cations and $[\text{Ni}(\text{dmit})_2]^-$ anions, typical of molecular conductors. Its structural arrangement is therefore not so comparable to that of **1**. On the contrary, the former resembles **1**, since it exhibits the same stoichiometry (one Fe complex and one Ni complex) but it also includes two solvent molecules. The magnetic properties of $[\text{Fe}(\text{qsal})_2][\text{Ni}(\text{dmit})_2] \cdot 2\text{CH}_3\text{CN}$ (named **1.solv.** hereafter) are totally different from that of **1**: it exhibits an almost complete spin transition around 230 K, and also a very small LIESST effect at low temperature [13]. The crystal structures of **1** and **1.solv.** are also clearly different¹: this is evidenced by

¹ The authors wish to thank K. Takahashi (Institute for Molecular Science and CREST, JST, Okazaki, Japan) for providing the cif file of **1.solv.**

(i) the packing of the $[\text{Ni}(\text{dmit})_2]^-$ anions, (ii) by the intramolecular geometry of the $[\text{Fe}(\text{qsal})_2]^+$ cations and (iii) by the packing of the $[\text{Fe}(\text{qsal})_2]^+$ cations.

- (i) Packing of the $[\text{Ni}(\text{dmit})_2]^-$ anions: in **1**, there are no short contacts between anions, whereas in **1-solv.**, anions pack along one-dimensional chains connected to each other through short $\text{S} \cdots \text{S}$ contacts.
- (ii) Intramolecular geometry of the $[\text{Fe}(\text{qsal})_2]^+$ cations: although the structure of **1-solv.** has been solved at 273 K, the bond lengths around Fe are larger than in **1**. Moreover, the discrepancies observed in **1** between ligands A and B are not present in **1-solv.** Whatever the ligand, for a given atom, the bond lengths are almost identical (Fe–O: 1.913 and 1.914 Å; Fe–N_{imine}: 2.125 and 2.138 Å; Fe–N_{quin.}: 2.150 and 1.151 Å for **1** and **1-solv.** respectively). On the contrary, in **1**, the Fe–N bond lengths are almost similar whatever be the nitrogen atom, except for one N atom of the quinoline ring in one of the qsal ligands: this length is much longer than the other ones. The distortion within the $\text{Fe}(\text{qsal})_2$ complex is also different in **1-solv.** and in **1**: the angles between the phenyl ring and the quinoline ring are almost similar in **1-solv.**: 8.65° and 7.58°, whereas they are very different in **1** (*ca.* 9° and 20°).
- (iii) Packing of the $[\text{Fe}(\text{qsal})_2]^+$ cations: alike in **1-solv.**, chains are also observed in **1**. However, a major difference between the two compounds lies in the relative orientation of the $[\text{Fe}(\text{qsal})_2]^+$ units: whereas several π – π interactions are observed in **1-solv.**, only short contacts between perpendicular ligands are observed in **1**. It is well established that π – π interactions are assumed to favour cooperativity in SCO complexes, and their occurrence in **1-solv.** explains that it exhibits an almost complete spin-transition, whereas **1** does not. The same conclusions can also be drawn by comparing **1** with $[\text{Fe}(\text{qsal})_2]\text{NCSe} \cdot \text{solvent}$ (solvent = MeOH, CH_2Cl_2 [11] or 2DMSO [12]): the latter exhibit complete spin transition and their structural arrangement presents π – π contacts between unsaturated rings of the $[\text{Fe}(\text{qsal})_2]^+$ cations.

Apparently, with the qsal ligand, the occurrence of π – π contacts between Fe cations seems to be the key point for the derived complexes to exhibit a complete spin-transition. In this line, the role of solvent has to be underlined: indeed, all 1:1 complexes based on $[\text{Fe}(\text{qsal})_2]^+$ but **1** are solvated. For instance, in **1-solv.**, acetonitrile is used for the metathesis reaction between the starting reagents and is finally included in the crystal structure. For **1**, the metathesis reaction takes place in a mixture of acetone and methanol, which are not included in the structure. In solvated complexes, the solvent molecule is connected to the qsal ligands via short contacts, and the resulting structural arrangement is a π stacking of the Fe complexes. One question still remains: what is responsible for that? Does the solvent induce the π stacking, or does the struc-

tural arrangement of the Fe complexes induce the position of the solvent? Whatever the answer, these subtle intra- and inter-molecular effects are difficult to control and predict.

4. Conclusion

Sample **1** exhibits a rather unusual magnetic behaviour with a very gradual change of the magnetic moment. Mössbauer spectra clearly show that the magnetic properties must be interpreted as an incomplete spin crossover of the iron(III) ions. Somewhat surprisingly, the application of external pressure does not allow changing the low-temperature residual high-spin fraction significantly. We infer that this residual fraction is not a thermally quenched metastable phase. The difference between the gradual spin crossover of **1** and the abrupt spin transition observed in **1-solv.** probably comes from the existence of π – π contacts between qsal ligands in the latter.

Acknowledgements

We thank COST D14, COST D35, the Picasso program (Acción Integrada HF2005-0117) and the Network of Excellence MagmaNet for financial support. J.A.R. thanks the Spanish Ministerio de Educacion y Ciencia (MEC) for the project CTQ 2004-03456/BQU. S. D. thanks the “Université Paul Sabatier” for an ATUPS grant during his Ph.D. position. J.-F. Meunier and A. Mari (LCC-CNRS) are acknowledged for technical assistance and M. Nardone (LNCMP, Toulouse) for the design of the high pressure cell.

Appendix A. Supplementary material

CCDC 628153, 628154 and 628155 contain the supplementary crystallographic data for this paper. These data can be obtained free of charge via <http://www.ccdc.cam.ac.uk/conts/retrieving.html>, or from the Cambridge Crystallographic Data Centre, 12 Union Road, Cambridge CB2 1EZ, UK; fax: (+44) 1223-336-033; or e-mail: deposit@ccdc.cam.ac.uk. Supplementary data associated with this article can be found, in the online version, at doi:10.1016/j.ica.2007.03.022.

References

- [1] P. Gütllich, H.A. Goodwin, Spin Crossover in Transition Metal Compounds I–III, Topics in Current Chemistry, 2004.
- [2] J.A. Real, A.B. Gaspar, M.C. Munoz, Dalton Trans. (2005) 2062.
- [3] O. Kahn, C. Martinez-Jay, Science 279 (1998) 44.
- [4] C. Faulmann, P. Cassoux, Prog. Inorg. Chem. 52 (2004) 399.
- [5] P. Cassoux, L. Valade, Inorganic Materials, second ed., 1996, 1.
- [6] S. Dorbes, L. Valade, J.A. Real, C. Faulmann, Chem. Comm. (2005) 69.
- [7] P.J. van Koningsbruggen, Y. Maeda, H. Oshio, Top. Curr. Chem. 233 (2004) 259.
- [8] B.M. Dahl, O. Dahl, Acta Chem. Scand. 23 (1969) 1503.

- [9] R.C. Dickinson, W.A. Baker Jr., R.L. Collins, J. Inorg. Nucl. Chem. 39 (1977) 1531.
- [10] H. Oshio, K. Kitazaki, J. Mishiro, N. Kato, Y. Maeda, Y. Takashima, J.C.S., Dalton Trans. (1987) 1341.
- [11] S. Hayami, Z.-z. Gu, H. Yoshiki, A. Fujishima, O. Sato, J. Am. Chem. Soc. 123 (2001) 11644.
- [12] S. Hayami, T. Kawahara, G. Juhasz, K. Kawamura, K. Uehashi, O. Sato, Y. Maeda, J. Radioanal. Nucl. Chem. 255 (2003) 443.
- [13] K. Takahashi, H. Cui, H. Kobayashi, E. Yasuaki, O. Sato, Chem. Lett. 34 (2005) 1240.
- [14] K. Takahashi, H.-B. Cui, Y. Okano, H. Kobayashi, Y. Einaga, O. Sato, Inorg. Chem. (2006).
- [15] G. Steimecke, H.J. Sieler, R. Kirmse, E. Hoyer, Phosphorus Sulfur 7 (1979) 49.
- [16] K.S. Varma, A.E. Underhill, Physica B+C: Physics of Condensed Matter 143 (1986) 321.
- [17] G. Molnár, T. Guillon, N.O. Moussa, L. Rechinat, T. Kitazawa, M. Nardone, A. Bousseksou, Chem. Phys. Lett. 423 (2006) 152.
- [18] F. Varret, in: International Conference on Mössbauer Effect Applications, Indian National Science Academy, New Delhi, Jaipur, India, 1981.
- [19] IPDS Software, version 2.86, Stoe, Darmstadt, Germany, 1996.
- [20] CrysAlis CCD, version 1.171.24, Xcalibur CCD system, Oxford Diffraction, 2004.
- [21] CrysAlis RED, version 1.171.24, Xcalibur CCD system, Oxford Diffraction, 2004.
- [22] A. Altomare, M.C. Burla, M. Camalli, G.L. Cascarano, C. Giacovazzo, A. Guagliardi, A.G.G. Moliterni, G. Polidori, R. Spagna, J. Appl. Cryst. 32 (1999) 115.
- [23] G.M. Sheldrick, SHELXS97 – A Program for Automatic Solution of Crystal Structure (Release 97–2), Göttingen, Germany, 1997.
- [24] G.M. Sheldrick, SHELXL97 – Programs for Crystal Structure Analysis (Release 97–2), Göttingen, Germany, 1998.
- [25] L.J. Farrugia, J. Appl. Cryst. 32 (1999) 837.
- [26] D.M. Watkin, L. Pearce, C.K. Prout, CAMERON – A Molecular Graphics Package, Chemical Crystallography Laboratory, University of Oxford, 1993.
- [27] L.J. Farrugia, J. Appl. Crystallogr. 30 (1997) 565.
- [28] T. Hahn (Ed.), International Tables for Crystallography, vol. A, Kluwer Academic Publishers, Dordrecht, The Netherlands, 1995.
- [29] A. Bousseksou, M. Verelst, H. Constant-Machado, G. Lemerrier, J.-P. Tuchagues, F. Varret, Inorg. Chem. 35 (1996) 110.
- [30] A. Thiel, A. Bousseksou, M. Verelst, F. Varret, J.P. Tuchagues, Chem. Phys. Lett. 302 (1999) 549.
- [31] A. Bousseksou, L. Salmon, F. Varret, J.P. Tuchagues, Chem. Phys. Lett. 282 (1998) 209.
- [32] N. Moliner, M.C. Munoz, S. Letard, L. Salmon, J.-P. Tuchagues, A. Bousseksou, J.A. Real, Inorg. Chem. 41 (2002) 6997.
- [33] V. Ksenofontov, A.B. Gaspar, P. Gütlich, Top. Curr. Chem. 235 (2004) 23.
- [34] A. Bondi, J. Phys. Chem. 68 (1964) 441.